Archean craton assembly and Paleoproterozoic accretion-collision tectonics in the Reguibat Shield, West African Craton

Dominique Chardon, Julien Berger, Florian Martellozzo

Precambrian Research 413 (2024) 107570

Contents lists available at ScienceDirect

Precambrian Research

journal homepage: www.elsevier.com/locate/precamres

Archean craton assembly and Paleoproterozoic accretion-collision tectonics in the Reguibat Shield, West African Craton

Dominique Chardon [*,1], Julien Berger, Florian Martellozzo

GET, Université de Toulouse, IRD, CNRS, UPS, CNES, Toulouse, France

ARTICLE INFO

Keywords:
Continental assembly
Continental growth
Accretion
Collision
Delamination
Peel-back orogen
Orocline
Siderian
Eburnean

ABSTRACT

Interpretation of the deformation pattern of the western Reguibat Shield by integrating current geochronological knowledge allows deciphering the assembly and post-assembly tectonic history of the Awsard craton that became involved in the giant Eburnean (~2 Ga) accretionary orogen. Final craton assembly took place along the newly recognized early Siderian (2.51–2.46 Ga) Tiris orogen. The eastern margin of the craton was then affected until 2.07–2.03 Ga by a west-verging (i.e., craton-ward) thrust system rooted in the collisional contact with the Eburnean orogen. Collision was controlled by thermal erosion and softening of the craton edge by the accretionary orogen, which allowed for the propagation of the thrust system during craton-ward progression of delamination of the cratonic lithospheric mantle. This resulted in the progressive incorporation of Archean crust into the accretionary orogen. Such a hot mode of collision provides a mechanism for the destruction of cratons by reworking of their crust into their flanking accretionary orogens and recycling of their lithospheric mantle into the asthenosphere. The hot collision mode favors the formation of specific oroclines driven by lithospheric mantle delamination.

1. Introduction

Cratons are nuclei of continental lithosphere that survived Late Precambrian and Phanerozoic geodynamics. The strong contrast in volumes of Archean continental crust between those predicted by continental growth models and those actually preserved in cratons implies crustal recycling or reworking (Cawood et al., 2013). The destruction of cratonic lithosphere must therefore have been effective throughout Earth history, and particularly during the Precambrian. How cratons were assembled and affected by, or incorporated into, younger orogens is key to investigate the fate of Archean lithosphere through Earth history. In the present study, we address the assembly and post-assembly deformation processes of the Archean cratons included in the West African Shield, also referred to as the West African Craton. The shield hosts two Archean provinces flanked by the giant Paleoproterozoic (~2.0 Ga) Eburnean-Transamazonian accretionary orogen (Fig. 1). Our work focuses on the tectonic interpretation of the deformation patterns of the Tiris complex, a > 200-km wide corridor forming the Archean-Eburnean collision zone in the northern part of the West African Craton known as the Reguibat Shield (Figs. 1 and 2). An assembly model is proposed for the Reguibat Shield, and a comparison with the Man-Léo shield (Fig. 1) allows reassessing the building history of the West African Archean lithosphere and refining a consumption model of Archean cratons by accretionary orogens.

2. Geological framework: The Tiris complex and its bounding terrains

The Tiris complex is bounded to the southwest by an Archean crustal province that has a NNE structural grain and consists mostly of TTG / granite-greenstone terrains of the Tasiast, Tichla, Tijirit and Amsaga domains (Rocci et al., 1991; Fig. 2). The main magmatic activity of the province that overlapped with regional granite-greenstone tectonics took place mostly between 2970 and 2920 Ma (Chardon, 1997; Key et al., 2008; Montero et al., 2014; Peucat and Chardon, unpublished SIMS and SHRIMP data). Old TTG gneisses (3025–3000 Ma) have been documented in the Tichla domain (Montero et al., 2014), whereas magmatic protoliths of the oldest gneisses of the province were dated in the Amsaga domain at 3530–3500 Ma and 3430–3410 Ma (Potrel et al., 1996). Latest tectonometamorphic activity along the NNE structural

* Corresponding author.
E-mail address: Dominique.chardon@ird.fr (D. Chardon).
[1] https://orcid.org/0000-0001-8439-2264.

https://doi.org/10.1016/j.precamres.2024.107570
Received 15 June 2024; Received in revised form 3 September 2024; Accepted 11 September 2024
Available online 24 September 2024

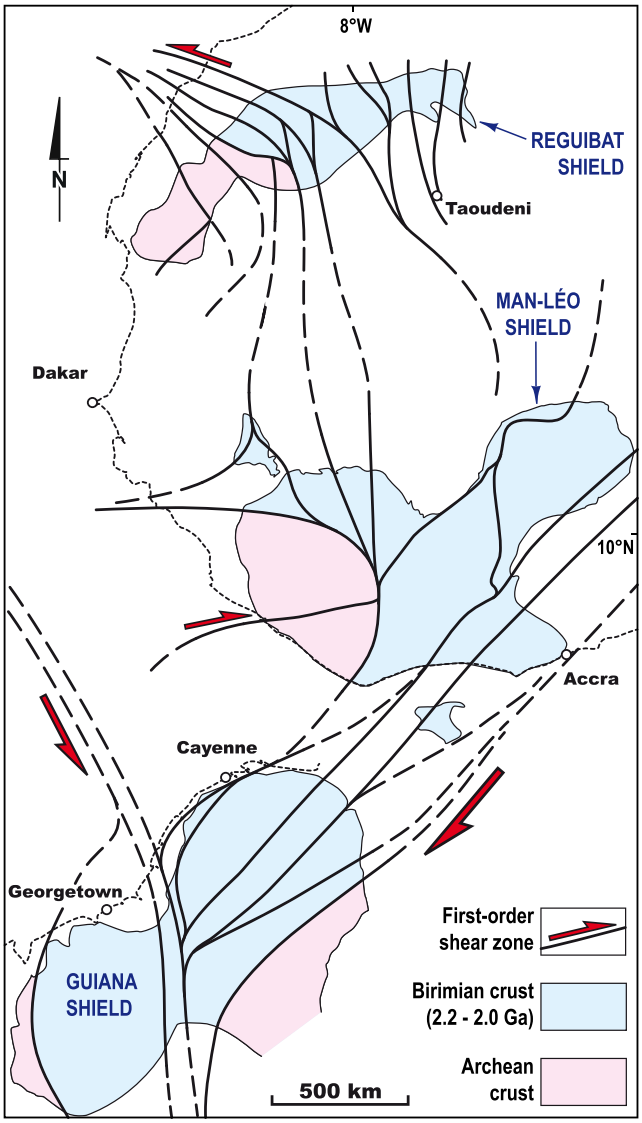

Fig. 1. Tectonic map of the Eburnean-Transamazonian accretionary orogen on a transatlantic reconstruction in the African reference frame (modified from Chardon et al., 2020; Traoré et al., 2022). The Man-Léo Shield and the Reguibat Shield are the two main outcrops of the West African Craton. Eburnean orogeny (2.15–2.01 Ga) affected pervasively the Birimian crust. Transamazonian is synonymous with Eburnean in South America.

grain of the province is attested to in the Amsaga domain by the emplacement of 2730–2720 Ma late/post-kinematic granitic and gabbroic plutons (Potrel et al., 1998, see also Key et al., 2008), which is consistent with emplacement of the undeformed Great Ahmeyin dike at 2730 Ma (Tait et al., 2013; Fig. 2). The Archean province SW of the Tiris complex therefore stabilized by that time. It is proposed to be named the AMTATI craton, an acronym for Amsaga / Tasiast / Tichla / Tijirit (Fig. 2). The NNE structural grain of the AMTATI craton and the Ahmeyin dike swarm are cut at a high angle by the Awsard fault, which forms the southwestern boundary of the Tiris complex (Fig. 2).

The Birimian crust was generated by granite-greenstone magmatism between ca. 2.2 and 2.0 Ga and constitutes the Eburnean accretionary orogen (Fig. 1). The Birimian crust that flanks the Tiris complex to the NE (Fig. 2) was magmatically accreted and reworked mostly between 2150 and 2100 Ma (Lahondère et al., 2003; Schofield et al., 2006; Combs, 2018). The area of investigation (red frame in Fig. 2) was chosen to encompass a significant part of that Birimian crust in order to decipher the potential relations between deformation of the western Eburnean orogen and that of Tiris complex.

The Tiris complex is an Archean high-grade terrain dominated by letpynites (leucogneisses), derived mostly from felsic volcanics and volcaniclastic series, which are interbedded with BIF (banded iron formation) layers (Rocci et al., 1991; Bronner et al., 1992). Leptynites show widespread evidence of partial melting and are intruded by anatectic granitic rocks. Most lithologies commonly show a granulitic overprint, attested to by the development of orthopyroxene (Opx) or garnet/cordierite-sillimanite assemblages in metasediments (Bronner, 1992). The age of the Tiris complex was loosely constrained to 2.70 – 2.63 Ga by only two Rb-Sr whole rock isochrons (Bronner, 1992, and references therein). It is only in the last decade that zircon U-Pb geochronology allowed for the documentation of two main plutonic episodes at 2.95–2.87 Ga and 2.69–2.65 Ga, while felsic plutonism and regional metamorphism were dated at 2.56–2.48 Ga in the southwestern part of the complex (Schofield et al., 2012; Lehbib, 2016).

3. Method

The desert environment is exceptionally propitious to photogeological mapping. The study area being located deep into the Sahara (e.g., Fig. 2), photointerpretation further allows for compensating its low accessibility, very low-relief outcrops, widespread reg cover, and a limited field-based documentation. Access to the Tiris complex is currently not permitted for security reasons. We therefore took advantage of the Google Earth™ software that allows for enhanced photointerpretation by combining the Shuttle Radar Topography Mission (SRTM) digital topography at 90 m resolution with an optimized satellite image cover. Following on from the monograph of Bronner (1992), we produced a new exhaustive and harmonized structural map of the Tiris complex and its margins (Fig. 2; Supplementary material, File S1). The map displays manually retrieved lithofabrics that represent the trace of geological layers, the most obvious and common ones being the BIF that contrast sharply with the letpynites. More generally, lithofabrics correspond to a banding underlined by amphibolite, quartzite, or marble layers and compositional contrasts within leptynites and gneisses (Bronner, 1992). That banding almost systematically coincides with the foliation measured in the field (Bronner, 1992; Fig. 3). Photointerpreted lithofabrics therefore approximate a composite planar fabric resulting from the transposition and recrystallization of the lithological layering into a foliation, which is common in high-grade terrains (Martelat et al., 2000). The deflection and alignment patterns of the fabrics allowed for the identification of the main shear zones and the kinematic interpretation of their horizontal component of slip (e.g., Martelat et al., 2000; Chardon et al., 2008; Fossen et al., 2022; Traoré et al., 2022; see Supplementary material, File S2). The resulting fabric / shear zone map (Fig. 4) reveals structural domains with specific fabric and shear zone patterns. In the following, these patterns are described and interpreted in the light of the available field-based documentation. Time constraints on their development are inferred from published LA-ICP-MS U-Pb results of Schofield et al. (2006, 2012), Lehbib (2016) and Combs (2018), which are listed in Table 1 and located on the structural map (Fig. 4).

4. Deformation and kinematics of the Archean – Paleoproterozoic collision zone

4.1. Domain A: Northeastern fringe of the AMTATI craton

The northeastern margin of the AMTATI craton has a NE structural grain intruded by a myriad of mafic dikes, most of which belonging to the Ahmeyin swarm (e.g., Lehbib, 2016). These dikes terminate against the Awsard fault, which marks the contact between the AMTATI craton and the Tiris complex (Fig. 4). The dikes are bent in a counterclockwise direction against the fault, which suggests a component of sinistral displacement along that fault.

4.2. Tiris complex

4.2.1. Domain B: Sheared terrain boundary

Domain B is an exception in the Tiris complex for it is very poor in BIF and is dominated by migmatitic sillimanite-cordierite paragneisses. It also hosts garnet leptynites, Opx-bearing and Opx-free TTG gneisses and porphyric granitic plutons (Bronner, 1992). Mineral assemblages are indicative of regional granulite facies metamorphic conditions at 600–850 °C and < 8 kbar (Schofield et al., 2012). The regional fabrics form an elongate zone of straight NW-trending trajectories flanking the Awsard fault. This zone is interpreted as a shear belt deflecting E-trending fabrics of the southeastern part of the domain in a clockwise direction (W of Agounit; Fig. 4). The overall fabric pattern suggests that the shear belt has a dextral component of slip and is rooted into a large-scale restraining bend in the Awsard fault. The apparent incompatibility between the dextral component of strike-slip in the shear belt and sinistral slip inferred along the Awsard fault may be due to reactivation of the southwestern edge of the shear belt, possibly during formation of the fault bend. Orthogneiss samples 7 and 8 (Fig. 4; Table 1) yielded magmatic protolith ages of 2473 ± 15 Ma and 2493 ± 17 Ma, respectively, whereas *syn*-kinematic granitic plutons (samples 6 and 1; Fig. 4; Table 1) yielded 2490 ± 19 Ma and 2472 ± 6 Ma, respectively. Considering errors in the ages and their overlaps, domain B must have undergone its main tectonomagmatic episode since ca. 2510 Ma, and its main tectonic activity between ca. 2480 and 2465 Ma.

4.2.2. Domain C: Shear-fold belt

Domain C hosts numerous BIF layers underlining a distinctive regional fold pattern. The domain also consists of Opx gneisses, amphibolites and felsic migmatites (Bronner, 1992). Antiforms are commonly cored by Opx gneisses and Opx granites, which underlay a distinctive regional BIF layer (the Féréouat bed), forming the base of a thick leptynite pile (Bronner, 1992). A first-order crustal layering therefore seems to have been preserved despite folding at high-grade conditions. Regional metamorphism has attained upper amphibolite facies conditions but relict granulite facies assemblages are widespread (e.g., Schofield et al., 2012).

At least three phases of folding have been distinguished locally (Bronner, 1992; Schofield et al., 2012). However, no regionally consistent superimposed fold patterns seems to apply to domain C. The fabric pattern reveals kilometer- to tens of kilometer-scale, doubly plunging elliptical antiforms and synforms with an overall NW trend (Figs. 4, 5a and 5b). Such patterns are compatible with type-1 fold interference patterns of Ramsay (1967). Antiforms and synforms are upright to steeply NE-dipping, with their axes plunging moderately (mostly) to steeply at their terminations (Fig. 5a and 5b). Map-scale curved axial traces are also common. Mineral lineations have generally a high pitch and therefore dominant steep plunges (Schofield et al., 2012; e.g., Fig. 5a). Fold packages are identified that define lens-shaped domains elongate in an overall NW-SE direction and separated by km-wide corridors of fabric trajectories defining an anastomosed network of shear zones (Fig. 4). The shear lenses defined by the shear network are mostly symmetrical, suggesting a bulk dominant coaxial regime in map view (Choukroune et al., 1987; Gapais et al., 1987). However, a few shear zones are through-going and rectilinear, with laterally consistent asymmetrical foliation patterns (sinistral shear zones trending E-W and a

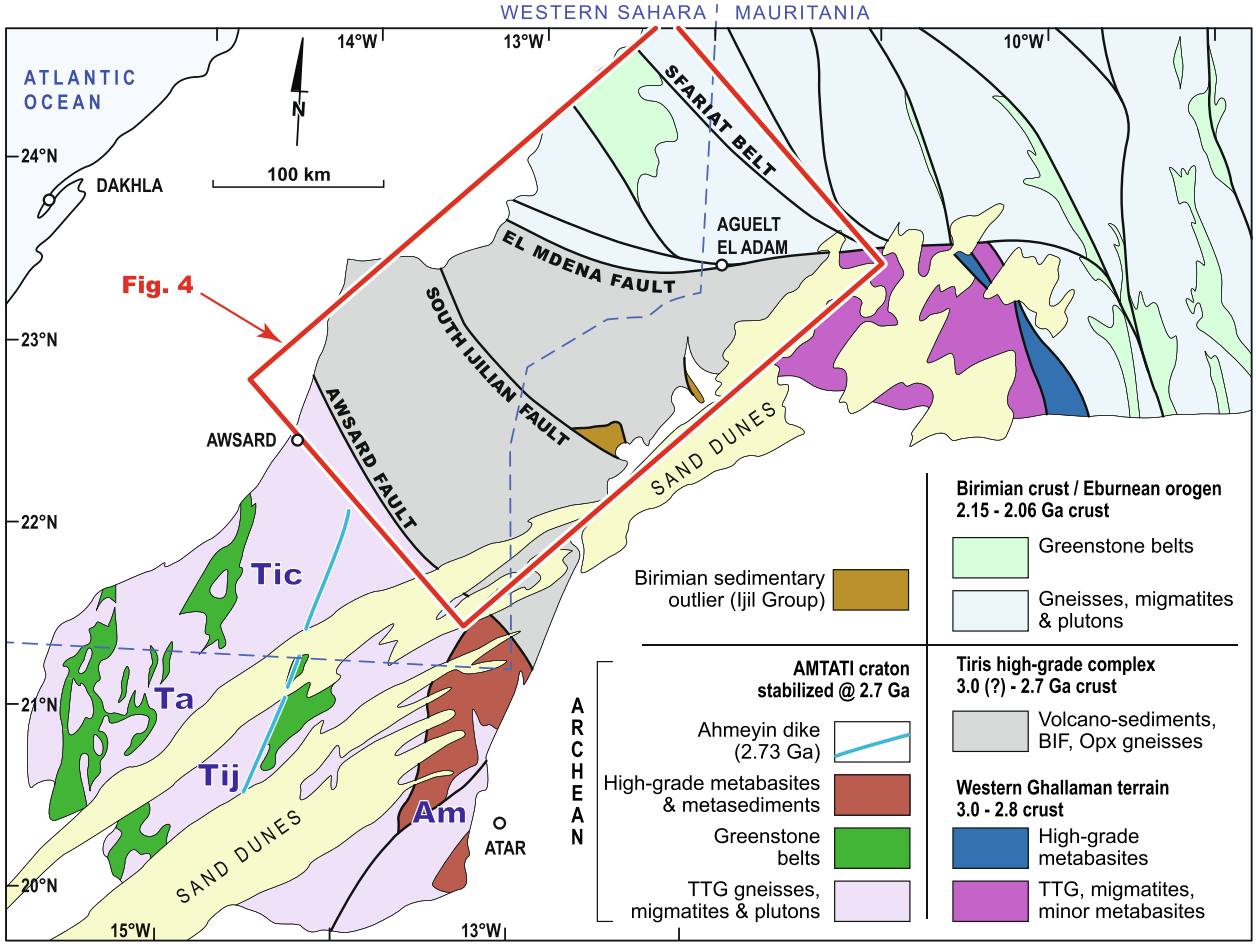

Fig. 2. Simplified geology of the western Reguibat Shield adapted from Bronner (1992) with modifications of the Archean-Paleoproterozoic boundary after Lahondère et al. (2003) and Combs (2018). Sub-domains of the AMTATI Craton: Ta – Tasiast, Tic – Tichla, Tij – Tijirit, Am – Amsaga.

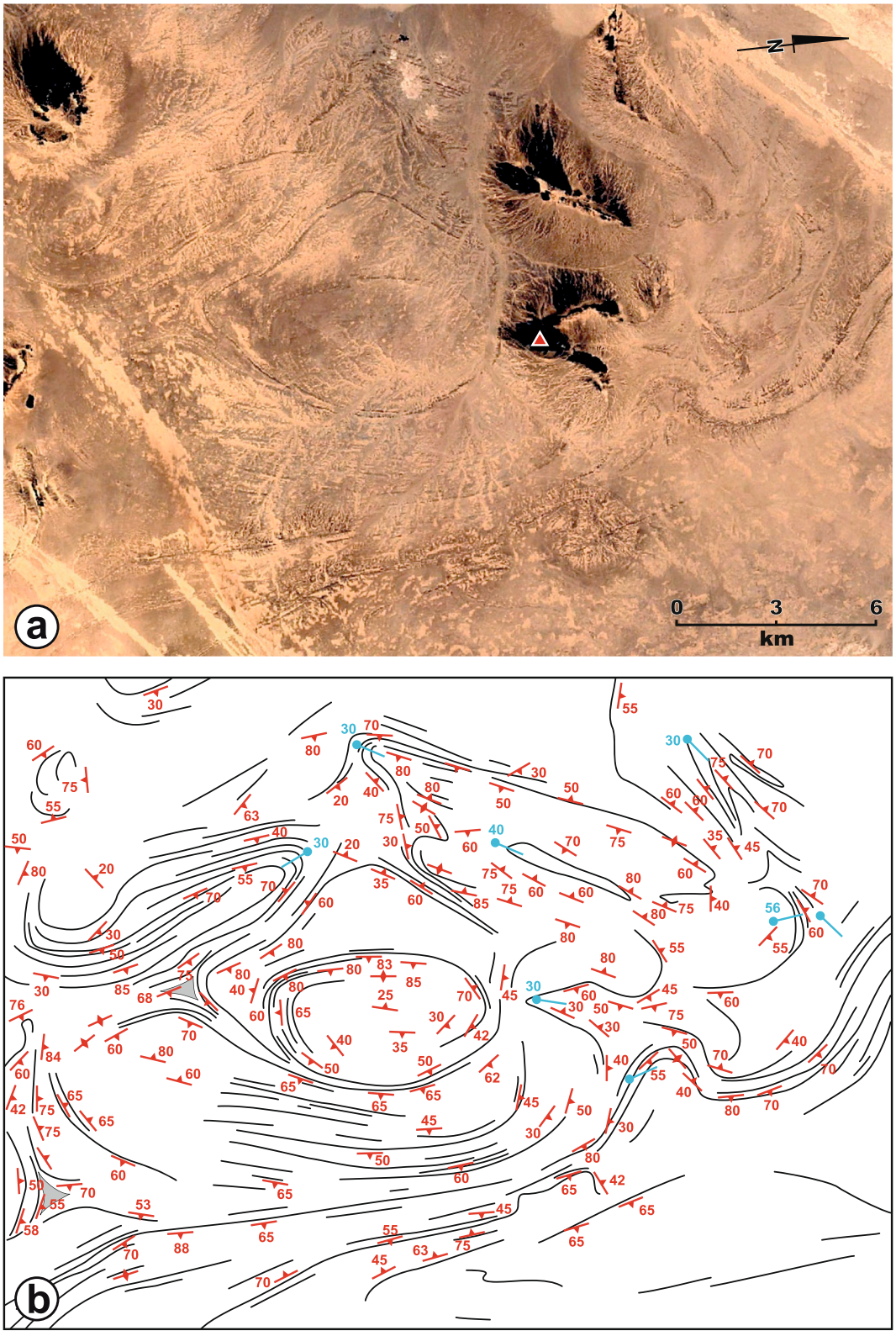

Fig. 3. Illustration of the structural mapping protocol. (a) Vertical aerial view of the area north of Fderik (© 2023 CNES / Airbus, © 2023 Maxar Technologies) (see Fig. 4 for location). (b) Corresponding raw photointerpreted lithofabrics from the present work and field structural measurements of Bronner (1992). Foliations in red and fold axes in blue. Coordinates of summit shown as a red triangle in (a): 22.9168°N/12.7300°W (511 m a.s.l.).

dextral one trending N-S; Fig. 4). The anastomozing shear zone pattern is deflected in a clockwise direction against its dextral shear boundary with domain B. The shear zone marking the boundary with domain D (the South Ijilian Fault; Bronner, 1992; Fig. 4) hosts steep mylonitic foliations and down-dip mineral-stretching lineations (Schofield et al., 2012).

A foliated garnet-bearing anatectic granite from the southeastern part of domain C provided a crystallization age of 2654 ± 8 Ma and a

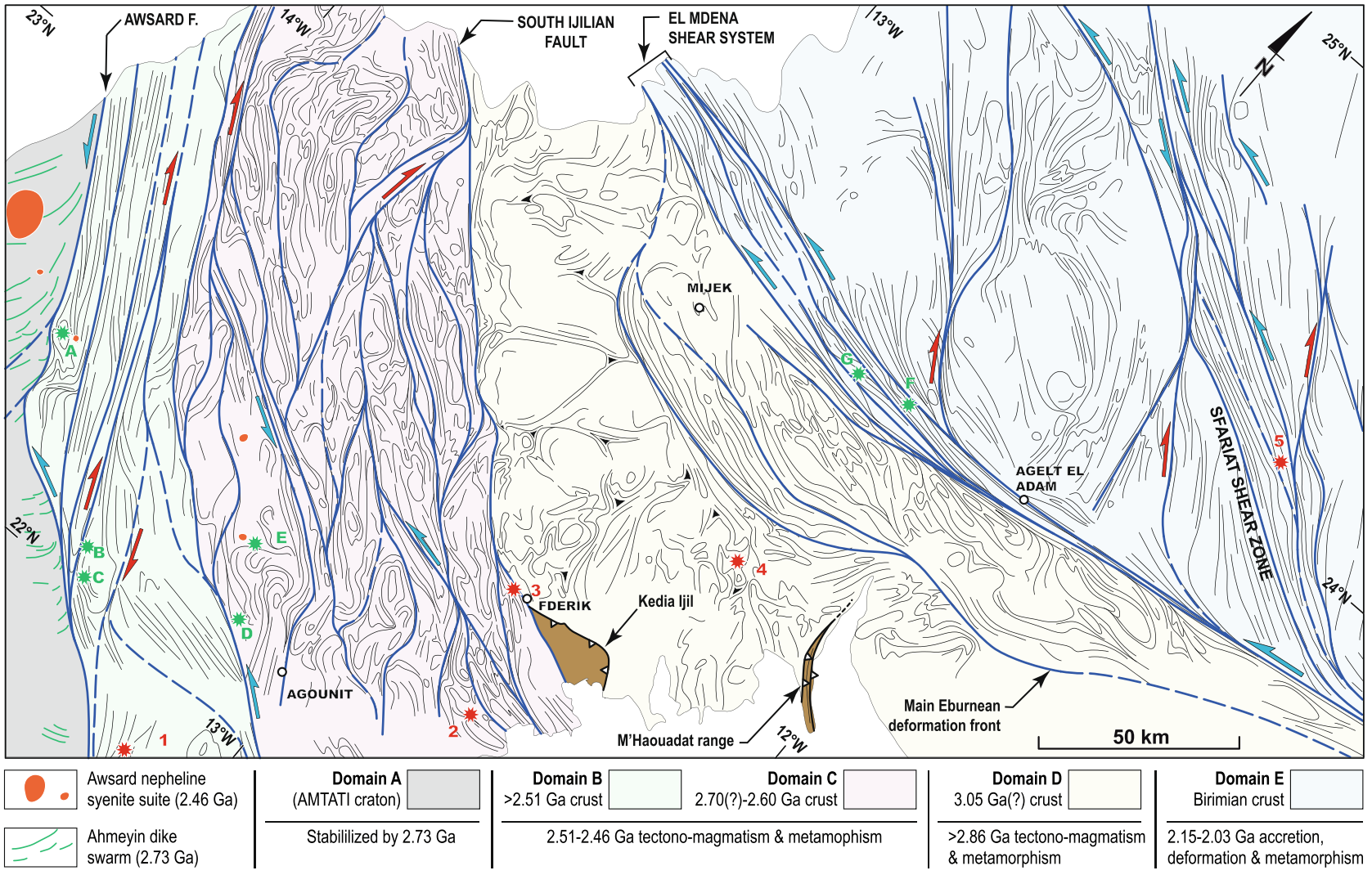

Fig. 4. Structural map of the Tiris complex (domains B to D) and its neighboring terrains (location on Fig. 2). Lithofabrics are in black; shear zones in blue; main foliation triple points (domain D) are shown as black triangles. Red and blue half arrows represent dextral and sinistral senses of shear, respectively. Birimian outliers of the Ijil Group are in brown. Red stars are the geochronological samples of Table 1. Sample 1 is located a few km southeast of the map frame. See supplementary material, File S1 for the raw photointerpreted lithofabrics and File S2 for a fabric map without the shear zones and structural domain boundaries.

Table 1
Summary of published U-Pb LA-ICP-MS dating results used to interpret the deformation patterns of the Archean-Paleoproterozoic collision zone in the Reguibat Shield (samples are located on Fig. 4).

Sample	Structural domain	Rock type	Age (Ma)	Method / Comment / interpretation	Reference
1	B	Syn-kinematic granitic pluton	2472 ± 6	U-Pb zircon, concordia age; crystallization age	a
2	C	Foliated garnet-bearing anatectic granite	2654 ± 8	U-Pb zircon, concordia age; age of anatexis	a
2	C	Foliated garnet-bearing anatectic granite	2482 ± 7	U-Pb monazite, concordia age; metamorphic age	a
3	C	Late-kinematic granitic dike	2487 ± 8	U-Pb zircon, concordia age; crystallization age; inherited zircons at 2550 and 2690 Ma	a
4	D	Fine-grained biotite-rich granite	2948 ± 11	U-Pb zircon, concordia age; crystallization age with ancient Pb-loss?	a
4	D	Fine-grained biotite-rich granite	2875 ± 18	U-Pb zircon, concordia age; crystallization age with crustal inheritance?	a
5	E	Foliated megacrystic granite hosted by mylonites	2064 ± 12	U-Pb zircon, upper intercept age; crystallization age	b
6	B	Alkaline granite	2490 ± 19	U-Pb zircon, upper intercept age; crystallization age.	c
7	B	Orthogneiss	2473 ± 15	U-Pb zircon, upper intercept age; magmatic protolith crystallization age	c
8	B	Orthogneiss	2493 ± 17	U-Pb zircon, upper intercept age; magmatic protolith crystallization age	c
9	C	Paragneiss	Age spectrum	U-Pb zircon; zircon population with age peaks at 3040, 2810, 2730 and 2530 Ma	c
10	C	Alkaline granite	2478 ± 23	U-Pb zircon, concordia age; crystallization age	c
11	E	Tonalite	2099 ± 15	U-Pb zircon, concordia age; crystallization age	c
12	E	Migmatitic gneiss	2100 ± 19	U-Pb zircon, concordia age; age of anatexis	d

a: Schofield et al. (2012); b: Schofield et al. (2006); c: Lehbib (2016); d: Combs (2018).

monazite metamorphic age of 2482 ± 7 Ma (sample 2; Fig. 4; Table 1). An alkaline granite (sample 10; Fig. 4; Table 1) is dated at 2478 ± 23 Ma, whereas a late-kinematic granitic dike from the northeastern shear boundary of the domain (South Ijilian Faut; Sample 3; Fig. 4; Table 1) provided a crystallization age of 2487 ± 8 Ma with two components of crustal inheritance at ca. 2550 and 2690 Ma. The zircon population from a granulitic paragneiss (sample 9; Fig. 4; Table 1) provided a wide age spectrum, with peaks at 2530, 2620, 2810 and 3040 Ma. Taken together, U-Pb ages indicate that domain C is made of a crust at least 2690 Ma old, which underwent plutonism around 2660–2645 Ma and at ca. 2550 Ma. The younger ages indicate that tectonometamorphism (crustal melting, metamorphism and shear zone activity) associated with the acquisition of the regional deformation patterns of domain C occurred between 2495 and 2475 Ma.

4.2.3. *Domaine D: A Mesoarchean terrain*

Domain D may be divided in two sub-domains. The southern sub-domain is bounded to the north by a shear zone called hereafter the main Eburnean deformation front (Fig. 4; see below). This sub-domain displays a spectacular photo-geological pattern of thick BIF layers interlayered with monotonous series of letpynites, quartzites, Opx gneisses and amphibolites (e.g., Fig. 3; Bronner, 1992). Regional granulite facies metamorphism was recorded by the BIF at around 700–750 °C and 9–10 kbar before local retrogression to amphibolite facies conditions (Cuney et al., 1975). BIF layers of the southeastern sub-domain delineate a dome-and-basin structural pattern (Fig. 4). Domes are elliptical and dominantly elongate in a NE or N direction. They range in great length from a few kilometers to more than 30 km for the largest one (SSW of Mijek; Fig. 4). Domes are flanked by pinched synforms and cascading folds, especially near and within map-scale fabric triple points marking interferences between domes (Bronner, 1992; Fig. 4). Interfering fold patterns between domes led to BIF layers repetition / accumulation in synforms and triple points (Bronner, 1992). The dome-and-basin pattern is typical of diapiric crustal overturn documented in archetypal Paleoarchean or Mesoarchean granite-greenstone terrains (Rocci et al., 1991; Bronner, 1992; see Choukroune et al., 1995; Bouhallier et al., 1995). A fine-grained granite coring a dome NE of Fderik representative of plutonism during late dome emplacement provided two U-Pb zircon age components i.e., either (i) crystallization at 2948 ± 11 Ma with an ancient lead loss or (ii) crystallization at 2875 ± 18 Ma with crustal inheritance (sample 4; Fig. 4; Table 1). Diapiric overturn and associated magmatism are therefore at least ca. 2860 Ma old.

The northern sub-domain (North of the main Eburnean deformation front and South of the El Mdena shear system; Fig. 4) preserves both BIF and non-ferruginous quartzites (Bronner, 1992). Its deformation pattern contrasts with that of the southeastern sub-domain. The dome-and-basin structures are transposed into E-W fabrics trending parallel to the El Mdena shear system in the southern part of the sub-domain (S and SW of Mijek), whereas a series of elliptical folds occupy the inner part of the sub-domain (Fig. 4). These folds are arranged in an *en-échelon* pattern against the El Mdena shear system. The folds (among which type-2 interference patterns of Ramsay, 1967) are deflected in a counter-clockwise direction and sheared along the shear system (Fig. 4). This, together with the systematic deflection patterns of fabrics within and along the margins of the El Mdena shear system attests to a sinistral component of horizontal slip (Fig. 4). The northern sub-domain is therefore interpreted to represent a portion of domain D onto which shear deformation at the boundary with the Birimian crust of domain E imprinted the Archean crust by reworking the > 2860 Ma dome-and-basin structural pattern.

The Kedia Ijil and the M'Haouadat Range are Birimian sedimentary outliers of the Ijil Group resting unconformably on the high-grade crust of domain D south of the main Eburnean deformation front (Figs. 2 and 4; Bronner, 1992). They consist mostly of greenschist to lower amphibolite facies BIF and micaschists whose age is loosely constrained by Rb-Sr and K-Ar whole-rock and mineral dating between 2.20 and

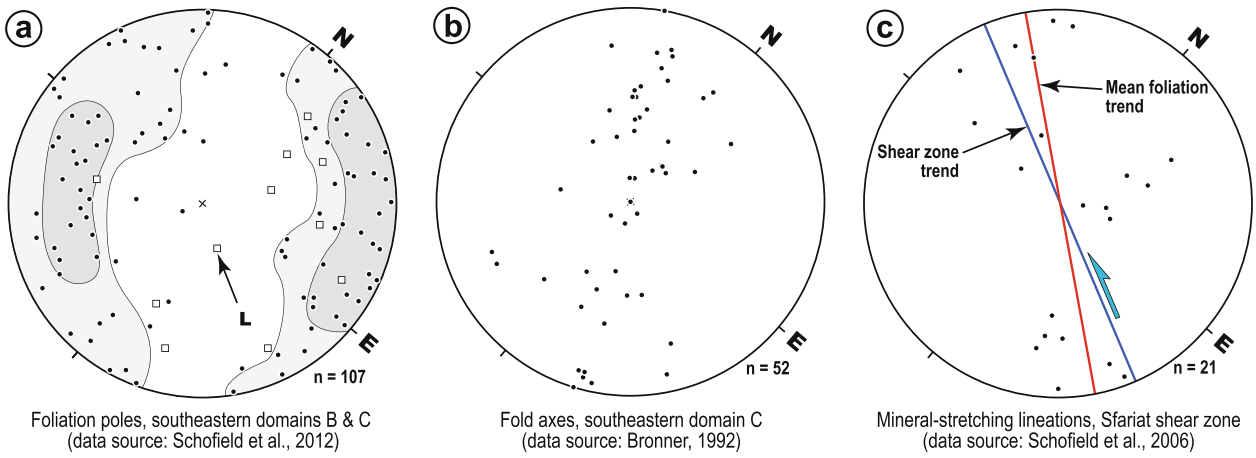

Fig. 5. Selected field structural data. (a) Foliation poles from the southeastern part of domains B and C (Fig. 4). Mineral-stretching lineations are shown as open squares (L). (b) Fold axes from the southeastern part of domain B (Fig. 4). (c) Mineral-stretching lineations from the Sfariat shear zone (domain E; Fig. 4). Sources for the data: Bronner (1992), Schofield et al. (2006, 2012). Stereonets are rotated clockwise so that they may be compared with the structural trends in Fig. 4 (equal area, lower hemisphere projection).

1.65 Ga (Bronner, 1992, and references therein). The Kedia Ijil is a half flower structure made of slivers thrust northeastwardly onto the Archean basement and affected by brittle-ductile NE-side up shearing along the South Ijilian Fault (Bronner, 1992; Fig. 4). The M'Haouadat Range is a sliver involved in a steep SW-verging reverse basement fault system (Bronner and Fourno, 1992; Fig. 4). The outliers are interpreted as remnants of a cover sequence that were trapped in structures that reactivated the cratonic foreland (i.e., domain D) of the Eburnean orogen beyond the main Eburnean deformation front (see also Schofield and Gillespie, 2007).

4.3. Birimian crust / Eburnean orogen (domain E)

The Birimian granite-greenstone terrain displays an overall NW-trending fabric / shear zone pattern, which is rooted into, and sinistrally deflected by, the El Mdena shear system (Fig. 4). The anastomosed and conjugate pattern of shear zones is typical of bulk inhomogeneous shortening documented throughout the Eburnean orogen in the Man-Léo Shield (Chardon et al., 2020; Traoré et al., 2022; Fig. 1). Within this pattern, the Sfariat shear zone is underlined by a corridor of shear-parallel, rectilinear fabrics up to 20-km-wide (Bronner, 1992; Fig. 4). Until U-Pb geochronological documentation of pervasive Birimian crust in between the El Mdena shear system and the Sfariat shear zone by Schofield et al. (2006), Lehbib (2016) and particularly Combs (2018), the shear zone (i.e., "Sfariat belt" on Fig. 2) was considered as the Eburnean suture zone between the Archean and Birimian crusts (Bronner, 1992). It must now be seen as part of the internal shear zone pattern of the Eburnean accretionary orogen (Figs. 2 and 3). Foliations are steeply NE-dipping to vertical in the shear zone and the mineral-stretching lineations are either steeply or shallowly plunging (Fig. 5c). Field-based shear criteria are either reverse or (mostly) sinistral (Schofield et al., 2006), which is consistent with left-lateral fabric deflection patterns within and at the margins of the shear zone (e.g., Fig. 4). The shear zone may be interpreted as having recorded partitioning between NE-side up and strike-slip shearing during sinistral transpression (see Tikoff and Greene, 1997; Gapais et al., 2005). Dextral shears antithetic to the Sfariat shear zone contributed to its boudinage (Fig. 4) in an overall kinematic framework of bulk inhomogeneous NE-directed shortening (e.g., Chardon et al., 2020; Traoré et al., 2022).

The Sfariat shear zone has recorded peak metamorphic conditions at around 800–900 °C and 7–10 kbar (Bronner, 1992). A foliated porphyric granite sheet involved in the shear zone's mylonites crystallized at 2064 ± 12 Ma (sample 5; Fig. 4; Table 1). This age overlaps with the monazite U-Th-Pb EMP age of 2038 ± 19 Ma obtained for a garnet-bearing granite sheet from the northeastern mylonitic wall of the shear zone by Lahondère et al. (2003). The Sfariat shear zone was therefore active after ca. 2075 Ma and no later than ca. 2020 Ma.

The El Mdena shear system (Fig. 4) is a corridor of steep shear zone networks preserving mylonites with steeply to shallowly plunging mineral-stretching lineations (Schofield et al., 2006). Given (i) its length (>250 km) and continuity, (ii) the ubiquitous left-lateral map kinematic patterns along its traces (Fig. 4), and (iii) the fact that it marks the southwestern limit of the Birimian crust, the El Mdena shear system is interpreted as the sinistral transpressional collisional boundary between the Eburnean orogen and the Archean crust. A migmatitic gneiss from the core of the shear system (sample 12; Fig. 4; Table 1) yielded an age of 2100 ± 19 Ma, which is consistent with the 2099 ± 15 Ma age of a neighboring tonalite (sample 11; Fig. 4; Table 1). These dates are only upper age constraints on the activity of the shear system. Nonetheless, late slip along the El Mdena shear system outlasted activity of the Sfariat shear zone (until after 2020 Ma?) and other shears in domain E for they are deflected along its trace (Fig. 4). In any case, sinistral transpressional kinematics of the El Mdena shear system is compatible and consistent with regional bulk inhomogeneous transpressional shortening recorded by the fabric / shear zone pattern of its Eburnean hinterland (domain E; Fig. 4).

5. Tectonic interpretation

5.1. The Tiris orogen: An early Siderian mobile belt in West Africa

Domains B and C are interpreted to form a single orogen, called hereafter the Tiris orogen (Fig. 6). Tectonomagmatism in the Tiris orogen started before 2510 Ma and lasted until ca. 2475 Ma, with later strain localization along the southwestern margin of the orogen (i.e., domain B) until ca. 2465 Ma. This timing is consistent with the age of 2460 ± 10 Ma obtained by Bea et al. (2013) for the anorogenic Awsard Syenite plutons that intruded both the AMTATI craton and the Tiris orogen (Fig. 4).

No crust older that 2.7 Ga is formerly documented in the Tiris orogen. However, neodymium model ages (T_{DM}) of 3.04 and 3.14 Ga in domain C (samples 2 and 3, respectively; Fig. 4; Schofield et al., 2012) could suggest involvement of a crust comparable to that of the Mesoarchean terrain (domain D). Similarly, a T_{DM} value of 2.9 Ga in domain B (sample 1; Fig. 4; Schofield et al., 2012) would be consistent with the reworking of AMTATI craton crust at the southwestern margin of the mobile belt.

The Tiris orogen absorbed convergence between the AMTATI craton,

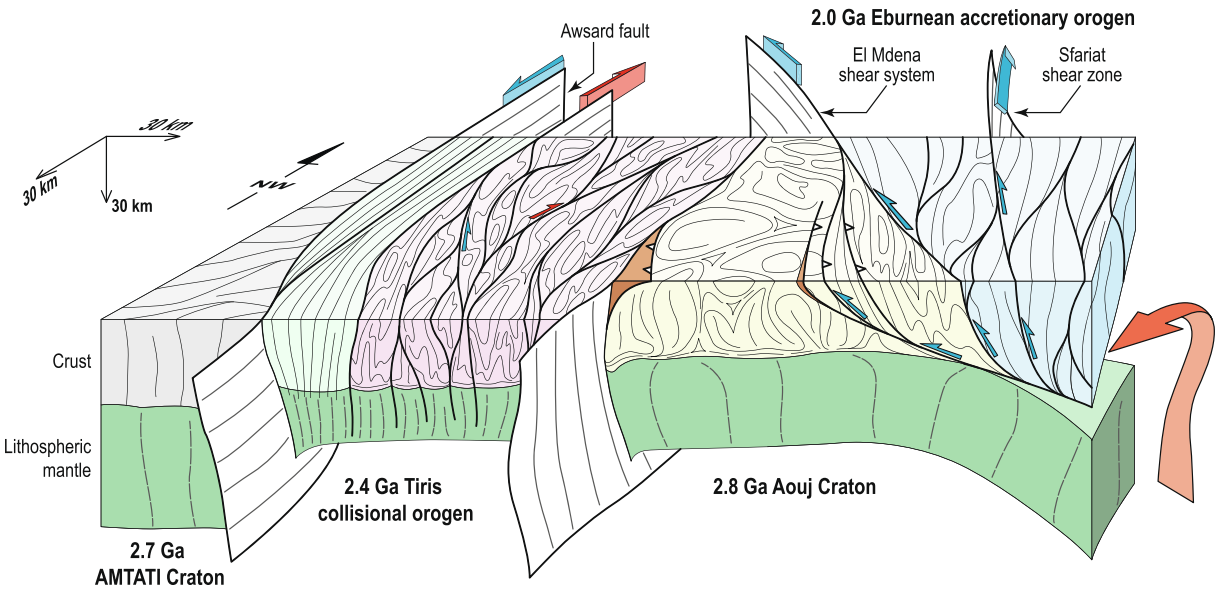

Fig. 6. Sketch structural model of the Archean-Paleoproterozoic collision zone of the Reguibat Shield at ca. 2.0 Ga. The large red arrow represents inferred asthenospheric corner flow.

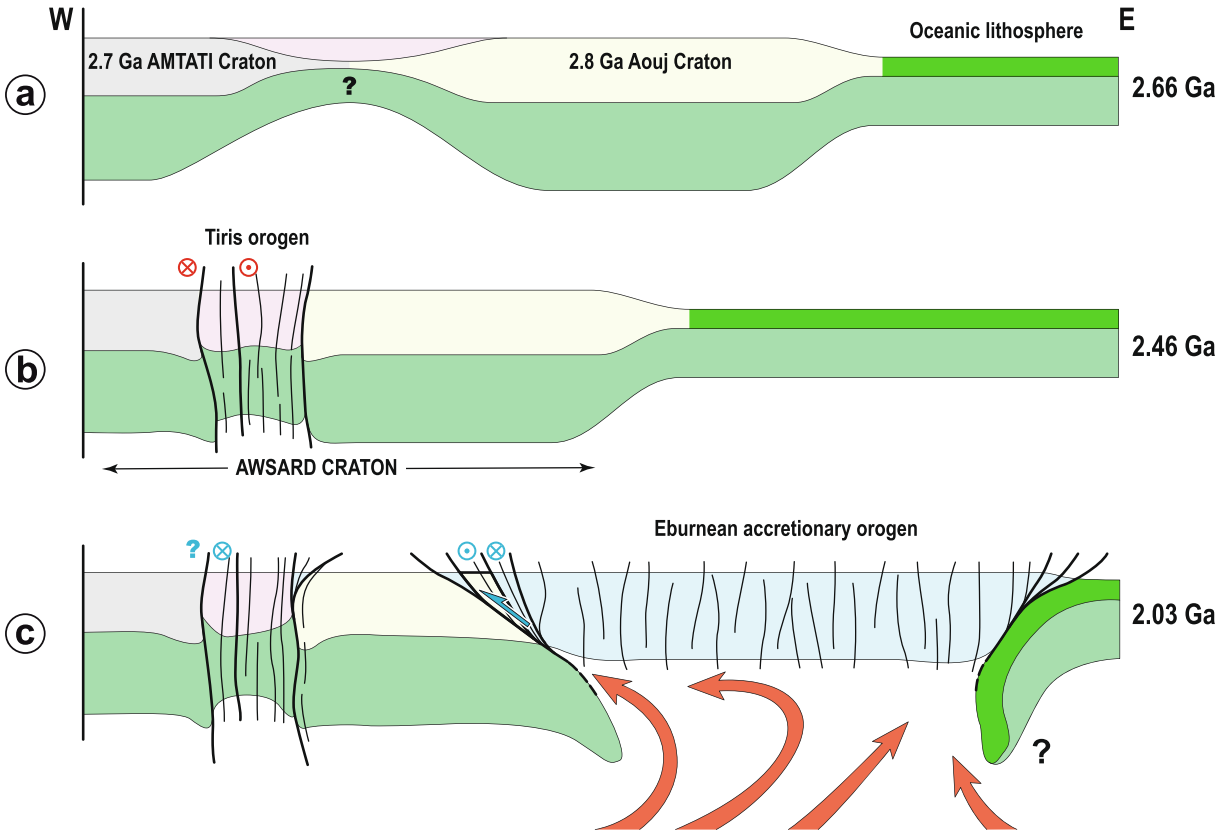

Fig. 7. Three-stage cross-sectional geodynamic model of the Reguibat Shield. (a) Hypothetical configuration at 2.66 Ga: a basin (rift?) has formed between the AMTATI Craton and the Aouj Craton. Whether such a basin installed on an earlier (>2.53 Ga) suture between the two cratons remains conjectural. (b) At 2.46 Ga, collision of the two cratons had formed the Tiris orogen. (c) At 2.03 Ga, the Aouj Craton has been partly consumed by propagation of collisional deformation at the rear (*retro*-side) of the Eburnean accretionary orogen and delamination of its mantle lithosphere. Collision tectonics reactivated structures of the foreland of the Eburnean orogen at least up to the eastern boundary of the Tiris orogen (South Igilian Fault). Red arrows are asthenospheric flow patterns. Note that the Eburnean orogen was wider than shown at the end of its construction (e.g., Fig. 1). The model considers a case in which consumption of the craton and delamination of its lithospheric mantle are commencing. The craton may have been wider, in which case the delaminated lithospheric slab would have been longer and a larger volume of its crust incorporated into the accretionary orogen. Note that the oceanic slab is shown in a configuration following its break-off. It could have been longer and continuous (e.g., Traoré et al., 2022).

stabilized after 2.73 Ga (domain A), and the Mesoarchean terrain formed by domain D. Orogenic deformation was partitioned between (i) bulk inhomogeneous shortening accommodated by large-scale folding and slip distribution through an anastomozing network of crustal-sale shear zones (domain C) and (ii) dextral shearing against the AMTATI craton (domain B). As a high-temperature mobile belt, the Tiris orogen would typically be a mixed hot orogen (Chardon et al., 2009). Sinistral slip along the southwestern orogenic front (Awsard fault) could be the record of the latest tectonic activity of the Tiris orogen or, more likely, a later reactivation.

5.2. The 2.8 Ga Aouj craton and its boundaries

Domain D represents an Archean craton that is distinct from the AMTATI craton (Fig. 6) and preserves regional diapiric dome-and-basin patterns at least 2860 Ma old. A potential crystalline basement for its volcano-sediments is not known. The T_{DM} of 3.25 Ga of sample 4 (Fig. 4; Table 1; Schofield et al., 2012) suggests that the craton hosts crust older than 2.86 Ga. Besides, the craton must include the Western Ghallaman terrain (Fig. 2; Schofield et al., 2006, 2012), where felsic plutonism took place around 3040 Ma (zircon TIMS age), 2930–2890 Ma (monazite EMP ages) and 2870–2830 Ma (zircon SHRIMP ages) (Lahondère et al., 2003). We propose to name this craton the Aouj Craton, with reference to the Aouj Formation (Bronner, 1992), which is several km thick and comprises major BIF layers that delineate the spectacular diapiric dome-and-basin structural pattern (Figs. 4 and 6). The craton is bounded by two diachronous orogenic belts (Fig. 6) i.e., the Tiris orogen to the SW and the Eburnean orogen to the NE.

The Tiris orogen has absorbed collision between the Aouj Craton and the AMTATI craton during the earliest Siderian i.e., between 2.51 and 2.46 Ga. The pre-orogenic configuration of the collision domain remains conjectural. It is tentatively interpreted as a (rift?) basin that received siliciclastic sediments from its western margin (protoliths of the paragneisses in domain B, with a maximal depositional age of 2530 Ma; sample 9, Table 1) and series of interbedded felsic volcano-sediments and BIF forming domain C (Figs. 4, 7a and 7b). Whether the Tiris orogen hosts a suture or reactivated a post-2.73 Ga, pre 2.53 Ga suture between the two cratons is even more hypothetical. The northeastern fringe of the Aouj Craton has been structurally reworked by the collision with the Eburnean accretionary orogen after ca. 2100 Ma (Fig. 6; see below).

5.3. Eburnean accretion-collision tectonics

The western margin of the Eburnean accretionary orogen is affected by anastomozing transpressional shears accommodating bulk inhomogeneous NE-directed shortening, which are rooted into its left-lateral, transpressive collisional contact with the Aouj Craton (i.e., the El Mdena shear system). Birimian magmatic accretion in this part of the orogen would have started around 2150 Ma (e.g., Combs, 2018), whilst regional transpression and final collision took place from ca. 2075 Ma and no later than ca. 2020 Ma.

The effect of Eburnean collision on the Aouj Craton is recorded by refolding and transposition of the Archean fabric patterns (Fig. 6). Transposition is best expressed behind the main Eburnean deformation front, whose arched map trace is suggestive of a thrust splay rooted in

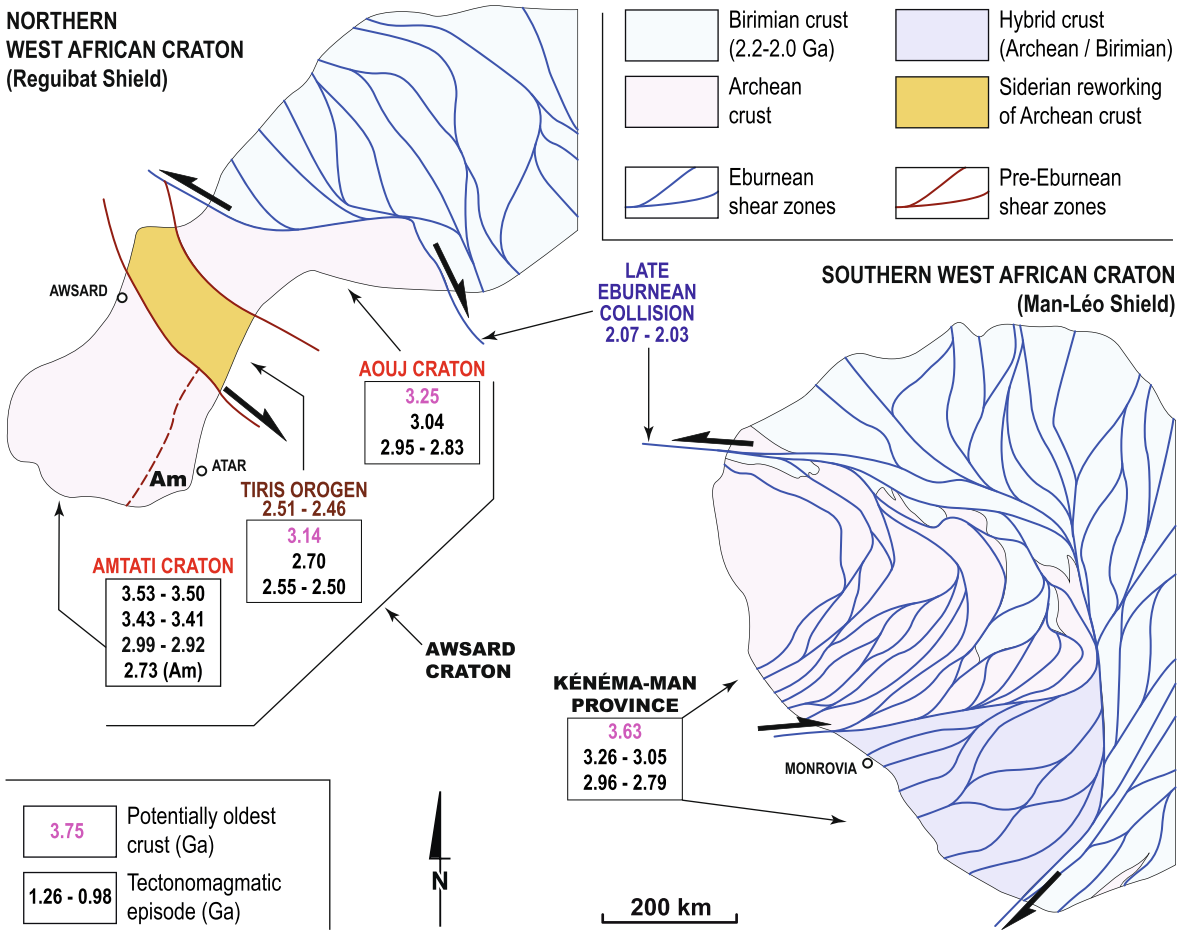

Fig. 8. Synoptic representation of the Archean crustal components of the West African craton and their relations to the Eburnean accretionary orogen (all ages in Ga). Structure of the southern West African craton is after Traoré et al. (2022) and its Archean ages after Rollinson (2016) and Koffi et al. (2020). Ages of potentially oldest crust are based on Nd model ages. Am – Amsaga. The two maps are not shown in their actual relative position (see Fig. 1).

the main collisional contact (Fig. 6). *En échelon* shear folding (of former Archean domes and basins?) took place closer to the contact (Fig. 6). In other words, superimposed structural patterns along the northeastern fringe of the craton attest to the imprint of Eburnean collisional fold-and-thrust deformation onto the craton (Fig. 6). South of the main Eburnean deformation front, collision affected the Archean basement along discreet transpressional and reverse fault structures such as the Kedia Ijil and the M'Haouadat range (Fig. 6). Along with the South Ijilian Fault (Fig. 6), shear zones of the 2.4 Ga Tiris orogen are likely to have been reactivated by the Eburnean collision. Latest sinistral slip along the Awsard fault could be a far-field effect of the Eburnean collision (Fig. 7c).

6. Discussion

6.1. Assembly of Archean cratons in West Africa

The present work allows for a redefinition of the main components and architecture of the Archean portion of the Reguibat Shield and its relations to the Eburnean accretionary orogen (Fig. 8). Correlations have been considered between the Reguibat Shield and the Man-Léo Shield, both from an Archean and Paleoproterozoic perspective (e.g., Rocci et al., 1991; Schofield et al., 2012; Grenholm et al., 2019). The Archean part of the Man-Léo Shield is called the Kénéma-Man province (Fig. 8). It is not strictly an Archean craton given the pervasiveness of Eburnean deformation overprint it has undergone (Traoré et al., 2022; Fig. 8). Beside this difference in Eburnean imprint, Archean correlations between the two shields are dubious for several reasons. Only one main episode of tectonomagmatism would match between the two shields i.e., at 2.96–2.92 Ga, in the AMTATI craton and the Kénéma-Man province, knowing that the two entities have contrasted histories before and after that period (Fig. 8). Importantly, the imprint of Siderian orogeny that ultimately sutured the AMTATI and Aouj cratons in the Reguibat Shield is not found in the Man-Léo Shield either. Finally, correlations of ill-dated Archean BIF bearing series inside the Reguibat Shield and between the Reguibat Shield and the Kénéman-Man province remain largely conjectural despite advances in geochronological dating (e.g., Bronner et al., 1992; Schofield et al., 2012). On the other hand, the transpressional character and the timing (2.07–3.03 Ga) of final collision between the Eburnean accretionary orogen and the Archean crust are strikingly similar in the two shields (present study; Traoré et al., 2022; e.g., Fig. 8), knowing that Eburnean accretionary magmatism and deformation started much earlier (e.g., at least 2150 Ma ago in the Western Reguibat Shield).

The Archean portion of the Reguibat Shield stabilized as a single craton after the Tiris orogeny at 2460 Ma. Given that the Awsard nephelinic intrusions seal orogenic stitching of the Aouj and AMTATI cratons on both sides of the Awsard fault, we propose to name it the Awsard Craton (Fig. 7, Fig. 8). The Kénéma-Man province and the Awsard Craton should be considered as separate entities that have evolved independently before being incorporated into the Eburnean accretionary orogen. This, together with the spatial and temporal assembly pattern of the Reguibat Shield (e.g., Fig. 8) should prompt further caution while attempting correlations between the West African Craton and the East European Craton such as those of Terentiev and Santosh (2020).

6.2. Fate of cratons during accretionary orogeny

The propagation pattern of Eburnean deformation onto the Awsard Craton provides clues on how cratons become reworked by younger accretionary orogens (Figs. 6 and 7). Despite their high strength and relative buoyancy (Poudjom Djomani et al., 2001), cratons may be thrust under the mostly juvenile, hot and highly buoyant crust of their flanking accretionary orogens as documented in the Reguibat and Man-Léo shields during Eburnean collision (present study; Feybesse and Milési, 1994). Given the asthenospheric fluxes generated under mature accretionary orogens that lack – by definition – an insulating lithospheric mantle (Chardon et al., 2009), the adjacent Archean lithospheric mantle is thermally eroded and/or weakens, allowing for heating of the crust, which can then deform at craton edge (Pitra et al., 2010, Traoré et al., 2022). Such fluxes eventually initiate craton-ward delamination of the lithospheric cratonic mantle, which is further enhanced by asthenospheric corner flow into the opening space between the Archean crust and its lithospheric mantle (Gray and Pysklywec, 2012; Traoré et al., 2022; e.g., Fig. 7c). Within such a geodynamic context, craton-ward thrust propagation is interpreted to mark the emergence of an inter-plate fault system rooted at the roof of the delaminating Archean lithospheric mantle (Figs. 6 and 7c). In a feed-back loop mechanism, delamination further enhances asthenospheric corner flow into the collision zone. This in turn allows for heat advection and mixing of newly formed Birimian crust and weakened Archean crust within and at the rear of the propagating thrust system (Figs. 6 and 7c). Such a model has been introduced to account for the Archean-Eburnean collision in the Man-Léo Shield, where the Eburnean shear zone pattern illustrates deep crustal collisional deformation in intricated Archean and Birimian crusts (Traoré et al., 2022; Fig. 8). In the Reguibat Shield, the Eburnean collisional fold-and-thrust propagation pattern into the Awsard craton would be compatible with incipient collision at mid / upper crustal levels (e.g., Fig. 6). Protracted craton-ward migration of the collision front accompanying delamination should eventually lead to the incorporation (reworking) of Archean crust into the accretionary orogen while the remaining cratonic lithospheric mantle sinks into the asthenosphere (Figs. 6 and 7c). In the Man-Léo Shield, such a reworking is compatible with the overall craton-ward younging pattern of Birimian magmatic accretion ages and increasing documentation of Archean inheritance or even Archean rocks in the Eburnean accretionary orogen (Traoré et al., 2022; see Grenholm et al., 2019). In the Reguibat Shield, Archean crustal inheritance at 2860–2780 Ma that started to be documented in the Birimian crust east of the Eburnean deformation front (Schofield et al., 2006) further supports such a model.

To summarize, the Archean-Paleoproterozoic collision zone in the West African Craton is a peel-back controlled orogen (Ueda et al., 2012; Chowdhury et al., 2020) forming the rear (i.e., *retro*-side) of a wide accretionary orogen that would be bounded on its pro-side by an oceanic subduction (Traoré et al., 2022; see Gray and Pysklywec, 2012; e.g., Fig. 7c). Ultimately, tectonic and magmatic growth of the accretionary orogen is controlled by subduction dynamics at its pro-side, delamination dynamics of the Archean lithosphere at its *retro*-side and their respective influence on asthenospheric flow patterns under the orogen. This model implies continent-ward growth of the accretionary orogen at the expense of its flanking craton.

The (sub)rounded convex map shape of the Archean-Birimian contact and its molding by the Eburnean structures in both the Reguibat and Man-Léo shields (Figs. 1 and 8) suggest that collision was accompanied by orocline bending (Johnston et al., 2013; see also Traoré et al., 2022). Instead of being a consequence of orocline bending (Gutiérrez-Alonso et al., 2004), delamination may be seen as the driver of orocline amplification. Indeed, the whole cratonic lithosphere is too strong to buckle around a vertical axis and the far-field shortening regime that is inferred to drive buckling cannot be readily substantiated (e.g., Rosenbaum, 2014). In our model, orocline bending would simply accompany craton-ward propagation of delamination concomitantly with incorporation of the Archean crust into the accretionary orogen (Fig. 9). Such a mechanism is markedly different from modern orocline bending resulting from oceanic slab retreat (e.g., Jolivet et al., 2006). In the latter case, the orocline grows against the slab dip direction and accompanies slab retreat by opening an extensional back arc domain. In three dimensions, the slab acquires a concave shape beneath the orocline. In our model (Fig. 9), the orocline grows towards the dip direction of the delaminating lithospheric mantle slab, which acquires a convex shape and dips away from the orocline (Fig. 9). But as for the modern slab

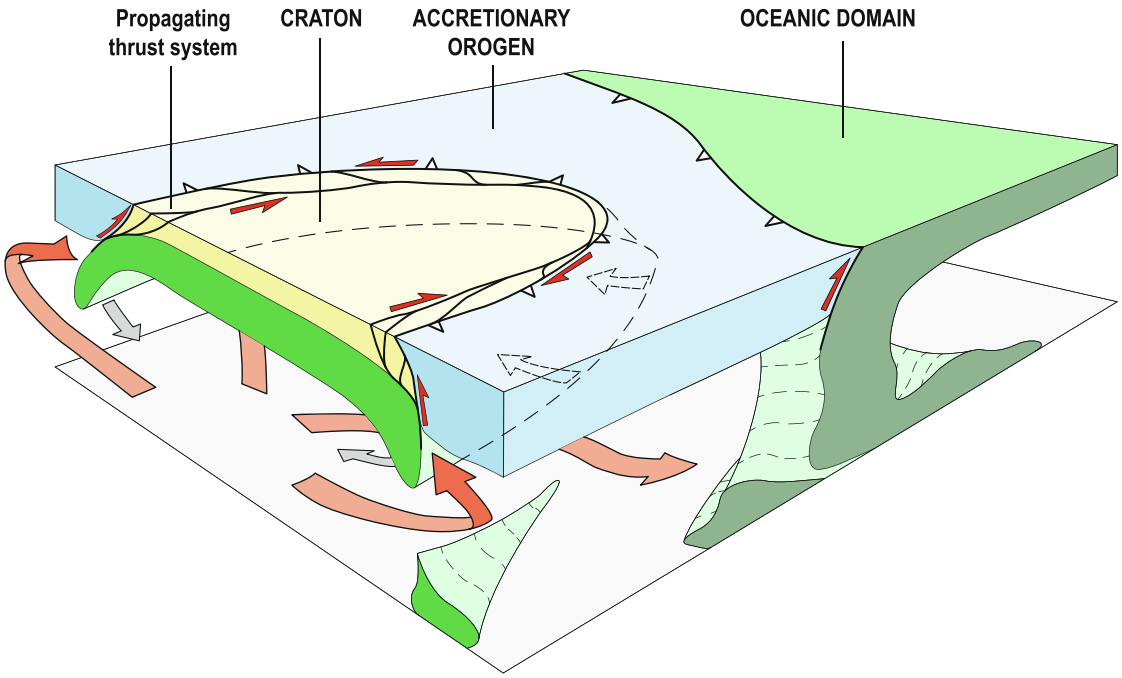

Fig. 9. Model of three-dimensional delamination driven collision between a craton and its adjoining accretionary orogen, as inspired by the examples of the West African craton. Large red arrows: asthenospheric flow patterns. Grey and dashed arrows: retreat / sinking of the cratonic lithospheric mantle.

retreat case, slab tear accompanied by strike-slip shearing would be a necessary condition for triggering and/or maintaining orocline growth (Jolivet et al. 2015; see Traoré et al., 2022). Magmatic growth, pervasive partial melting and general flow of the accretionary orogen (Chardon et al., 2009) would fill up the space generated by *retro*-delamination and compensate for the incorporation of Archean crust into the accretionary orogen (Fig. 9). Such oroclines may be common in Precambrian accretionary orogens (e.g., Corrigan et al., 2021). The delamination-driven orocline growth model provides a mechanism for reworking large volumes of cratonic crust in accretionary orogens and recycling mantle lithosphere into the asthenosphere.

7. Conclusion

In the Reguibat Shield, the collision zone between the Eburnean accretionary orogen and the 2.7 Ga AMTATI craton consists of a Mesoarchean craton i.e., the Aouj Craton. This craton collided southwestward with the AMTATI craton along a newly documented HT mobile belt, the Tiris orogen, in the early Siderian (2.51–2.47 Ga), and was later affected along its northeastern margin by the Eburnean collision until 2.07–2.03 Ga. The Tiris orogeny achieved the final assembly of the Archean components of the Reguibat Shield to build the Awsard Craton. This craton is distinct from the Archean part of the southern West African Craton (Man-Léo Shield), but the two paleocontinents were involved in a same way in the Eburnean collision.

Eburnean collision is interpreted to have been mainly controlled by the thermal impact of the accretionary orogen on the cratons edge. It combined backward delamination of the Archean lithospheric mantle and craton-ward fold-and-thrust propagation of Eburnean deformation, which led to the incorporation of Archean crust into the accretionary orogen. Such a process contributes to rework the Archean crust into its flanking accretionary orogen and the thermal erosion, destruction and sinking of the Archean lithospheric mantle into the asthenosphere. Hot collision of accretionary orogens with cratons would form specific oroclines driven by cratonic lithospheric mantle delamination.

CRediT authorship contribution statement

Dominique Chardon: Writing – original draft, Validation, Supervision, Methodology, Investigation, Conceptualization. **Julien Berger:** Writing – review & editing, Validation, Supervision, Investigation. **Florian Martellozzo:** Visualization, Investigation, Formal analysis.

Declaration of competing interest

The authors declare that they have no known competing financial interests or personal relationships that could have appeared to influence the work reported in this paper.

Data availability

The raw lithofabric map produced for the present study is availble as supplementary file S1 in kml format.

Acknowledgements

We thank Quentin Masurel and an anonymous referee for their constructive reviews of the manuscript.

Appendix A. Supplementary data

Supplementary data to this article can be found online at https://doi.org/10.1016/j.precamres.2024.107570.

References

Bea, F., Montero, P., Haissen, F., El Archi, A., 2013. 2.46 Ga kalsilite and nepheline syenites from the Awsard pluton, Reguibat Rise of the West African Craton, Morocco. Generation of extremely K-rich magmas at the Archean-Proterozoic transition. Precambr. Res. 224, 242–254. https://doi.org/10.1016/j.precamres.2012.09.024.

Bouhallier, H., Chardon, D., Choukroune, P., 1995. Strain patterns in Archaean dome-and-basin structures: the Dharwar craton (Karnataka, South India). Earth Planet. Sci. Lett. 135, 57–75. https://doi.org/10.1016/0012-821X(95)00144-2.

Bronner, G., 1992. Structure et évolution d'un craton archéen. La dorsale Reguibat occidentale (Mauritanie). Tectonique et métallogénie des formations ferrifères. Doc. BRGM 201, 1–448.

Bronner, G., Chauvel, J.-J., Triboulet, C., 1992. Les formations ferrifères du Précambrien de Mauritanie: origine et évolution des quartzites ferrugineux. Chron. Rech. Min. 508, 3–27.
Bronner, G., Fourno, J.P., 1992. Audio-magnetotelluric investigation of allochthonous iron formations in the Archaean Reguibat shield (Mauritania): structural and mining implications. J. Afr. Earth Sc. 15, 341–351. https://doi.org/10.1016/0899-5362(92)90019-9.
Cawood, P.A., Hawkesworth, C.J., Dhuime, B., 2013. The continental record and the generation of continental crust. Geol. Soc. Am. Bull. 125, 14–32. https://doi.org/10.1130/B30722.1.
Chardon, D., Jayananda, M., Chetty, T.R.K., Peucat, J.-J., 2008. Precambrian continental strain and shear zone patterns: South Indian case. J. Geophys. Res. 113, B08402. https://doi.org/10.1029/2007JB005299.
Chardon, D., Gapais, D., Cagnard, F., 2009. Flow of ultra-hot orogens: A view from the Precambrian, clues for the Phanerozoic. Tectonophysics 477, 105–118. https://doi.org/10.1016/j.tecto.2009.03.008.
Chardon, D., Bamba, O., Traoré, K., 2020. Eburnean deformation pattern of Burkina Faso and the tectonic significance of shear zones in the West African craton. BSGF - Earth Sci. Bull. 191, 2. https://doi.org/10.1051/bsgf/2020001.
Chardon, D., 1997. Les déformations continentales archéennes : exemples naturels et modélisation thermomécanique. Mém. Géosciences Rennes 76, 1–257. https://theses.hal.science/tel-00619433.
Choukroune, P., Gapais, D., Merle, O., 1987. Shear criteria and structural symmetry. J. Struct. Geol. 9, 525–530. https://doi.org/10.1016/0191-8141(87)90137-4.
Choukroune, P., Bouhallier, H., Arndt, N.T., 1995. Soft lithosphere during periods of Archaean crustal growth or crustal reworking. Spec. Publ. Geol. Soc. 95, 67–86. https://doi.org/10.1144/GSL.SP.1995.095.01.05.
Chowdhury, P., Chakraborty, S., Gerya, T.V., Cawood, P.A., Capitanio, F.A., 2020. Peel-back controlled lithospheric convergence explains the secular transitions in Archean metamorphism and magmatism. Earth Planet. Sci. Lett. 538, 116224 https://doi.org/10.1016/j.epsl.2020.116224.
Combs, J., 2018. Geological and metallogenic evolution of the Palaeoproterozoic Adam Ahmed Mouloude region of the Reguibat shield, Western Sahara (PhD Thesis). Oxford University, Oxford. https://ora.ox.ac.uk/objects/uuid:7a059394-45e2-4c8c-bd4f-f3bfff83a27b.
Corrigan, D., Van Rooyen, D., Wodicka, N., 2021. Indenter tectonics in the Canadian Shield: a case study for Paleoproterozoic lower crust exhumation, orocline development, and lateral extrusion. Precambr. Res. 355, 106083 https://doi.org/10.1016/j.precamres.2020.106083.
Cuney, M., Bronner, G., Barbey, P., 1975. Les paragenèses catazonales des quartzites à magnétite de la province ferrifère du Tiris (Précambrien de la Dorsale Reguibat, Mauritanie). Pétrologie 1–2, 103–120. (reprinted in Bronner, 1992).
Feybesse, J.-L., Milési, J.-P., 1994. The Archaean/Proterozoic contact zone in West Africa: a mountain belt of décollement thrusting and folding on a continental margin related to 2.1 Ga convergence of Archaean cratons? Precambr. Res. 69, 199–227. https://doi.org/10.1016/0301-9268(94)90087-6.
Fossen, H., Harris, L.B., Cavalcante, C., Archanjo, C.J., Ávila, C.F., 2022. The Patos-Pernambuco shear system of NE Brazil: Partitioned intracontinental transcurrent deformation revealed by enhanced aeromagnetic data. J. Struct. Geol. 158, 104573 https://doi.org/10.1016/j.jsg.2022.104573.
Gapais, D., Balé, P., Choukroune, P., Cobbold, P.R., Mahjoub, Y., Marquer, D., 1987. Bulk kinematics from shear zone patterns: some field examples. J. Struct. Geol. 9, 635–646. https://doi.org/10.1016/0191-8141(87)90148-9.
Gapais, D., Potrel, A., Machado, N., Hallot, E., 2005. Kinematics of long-lasting Paleoproterozoic transpression within the Thompson Nickel Belt, Manitoba, Canada. Tectonics 24, TC3002. https://doi.org/10.1029/2004TC001700.
Gray, R., Pysklywec, R.N., 2012. Geodynamic models of mature continental collision: Evolution of an orogen from lithospheric subduction to continental retreat/delamination. J. Geophys. Res. Solid Earth 117, B03408. https://doi.org/10.1029/2011JB008692.
Grenholm, M., Jessell, M., Thébaud, N., 2019. A geodynamic model for the Paleoproterozoic (ca. 2.27–1.96 Ga) Birimian Orogen of the southern West African Craton – Insights into an evolving accretionary-collisional orogenic system. Earth Sci. Rev. 192, 138–193. https://doi.org/10.1016/j.earscirev.2019.02.006.
Gutiérrez-Alonso, G., Fernández-Suárez, J., Weil, A.B., 2004. Orocline triggered lithospheric delamination. Geol. Soc. Am. Spec. Pap. 383, 121–130. https://doi.org/10.1130/0-8137-2383-3(2004)383[121:OTLD]2.0.CO;2.
Johnston, S.T., Weil, A.B., Gutierrez-Alonso, G., 2013. Oroclines: Thick and thin. Geol. Soc. Am. Bull. 125, 643–663. https://doi.org/10.1130/B30765.1.
Jolivet, L., Augier, R., Robin, C., Suc, J.-P., Rouchy, J.M., 2006. Lithospheric-scale geodynamic context of the Messinian salinity crisis. Sedim. Geol. 188–189, 9–33. https://doi.org/10.1016/j.sedgeo.2006.02.004.
Jolivet, L., Menant, A., Sternai, P., Rabillard, A., Arbaret, L., Augier, R., Laurent, V., Beaudoin, A., Grasemann, B., Huet, B., Labrousse, L., Le Pourhiet, L., 2015. The geological signature of a slab tear below the Aegean. Tectonophysics 659, 166–182. https://doi.org/10.1016/j.tecto.2015.08.004.
Key, R.M., Loughlin, S.C., Gillespie, M., Del Rio, M., Horstwood, M.S.A., Crowley, Q.G., Darbyshire, D.P.F., Pitfield, P.E.J., Henney, P.J., 2008. Two Mesoarchaean terranes in the Reguibat shield of NW Mauritania. Spec. Publ. Geol. Soc. 297, 33–52. https://doi.org/10.1144/SP297.3.
Koffi, G.-R.-S., Kouamelan, A.N., Allialy, M.E., Coulibaly, Y., Peucat, J.-J., 2020. Re-evaluation of Leonian and Liberian events in the geodynamical evolution of the Man-Leo Shield (West African Craton). Precambr. Res. 338, 105582 https://doi.org/10.1016/j.precamres.2019.105582.
Lahondère, D., Roger, J., Thiéblemont, D., Goujou, J.-C., Marchand, J., Le Métour, J., 2003. Notice explicative des cartes géologiques et métallogéniques à 1/200 000 et 1/500 000 du Nord de la Mauritanie. Volume 1 - Géologie. Ministère des Mines et de l'Industrie, BRGM, Nouakchott.
Lehbib, N.S., 2016. Estudio geológico y metalogenético del basemento precámbrico del Sáhara Occidental (PhD Thesis). Universitat de Barcelona, Barcelona. https://diposit.ub.edu/dspace/handle/2445/110062?mode=full.
Martelat, J.-E., Lardeaux, J.-M., Nicollet, C., Rakotondrazafy, R., 2000. Strain pattern and late Precambrian deformation history in southern Madagascar. Precambr. Res. 102, 1–20. https://doi.org/10.1016/S0301-9268(99)00083-2.
Montero, P., Haissen, F., El Archi, A., Rjimati, E., Bea, F., 2014. Timing of Archean crust formation and cratonization in the Awsard-Tichla zone of the NW Reguibat Rise, West African Craton: A SHRIMP, Nd–Sr isotopes, and geochemical reconnaissance study. Precambr. Res. 242, 112–137. https://doi.org/10.1016/j.precamres.2013.12.013.
Pitra, P., Kouamelan, A.N., Ballèvre, M., Peucat, J., 2010. Palaeoproterozoic high-pressure granulite overprint of the Archean continental crust: evidence for homogeneous crustal thickening (Man Rise, Ivory Coast). J. Metam. Geol. 28, 41–58. https://doi.org/10.1111/j.1525-1314.2009.00852.x.
Potrel, A., Peucat, J.J., Fanning, C.M., Auvray, B., Burg, J.P., Caruba, C., 1996. 3.5 Ga old terranes in the West African Craton, Mauritania. J. Geol. Soc. 153, 507–510. https://doi.org/10.1144/gsjgs.153.4.0507.
Potrel, A., Peucat, J.J., Fanning, C.M., 1998. Archean crustal evolution of the West African Craton: example of the Amsaga Area (Reguibat Rise). U-Pb and Sm-Nd evidence for crustal growth and recycling. Precambr. Res. 90, 107–117. https://doi.org/10.1016/S0301-9268(98)00044-8.
Poudjom Djomani, Y.H., O'Reilly, S.Y., Griffin, W.L., Morgan, P., 2001. The density structure of subcontinental lithosphere through time. Earth Planet. Sci. Lett. 184, 605–621. https://doi.org/10.1016/S0012-821X(00)00362-9.
Ramsay, J.G., 1967. Folding and fracturing of rocks. MacGraw-Hill, New York.
Rocci, G., Bronner, G., Deschamps, M., 1991. Crystalline basement of the West African craton, in: Dallmeyer, R.D., Lécorché, J.-P. (Eds.), The West African Orogens and Circum-Atlantic Correlatives. Springer-Verlag, Berlin, pp. 31–61.
Rollinson, H., 2016. Archaean crustal evolution in West Africa: A new synthesis of the Archaean geology in Sierra Leone, Liberia, Guinea and Ivory Coast. Precambrian Res. 281, 1–12. https://doi.org/10.1016/j.precamres.2016.05.005.
Rosenbaum, G., 2014. Geodynamics of oroclinal bending: Insights from the Mediterranean. J. Geodyn. 82, 5–15. https://doi.org/10.1016/j.jog.2014.05.002.
Schofield, D.I., Gillespie, M.R., 2007. A tectonic interpretation of "Eburnean terrane" outliers in the Reguibat Shield, Mauritania. J. Afr. Earth Sci. 49, 179–186. https://doi.org/10.1016/j.jafrearsci.2007.08.006.
Schofield, D.I., Horstwood, M.S.A., Pitfield, P.E.J., Crowley, Q.G., Wilkinson, A.F., Sidaty, H.C.O., 2006. Timing and kinematics of Eburnean tectonics in the central Reguibat Shield, Mauritania. J. Geol. Soc. 163, 549–560. https://doi.org/10.1144/0016-764905-097.
Schofield, D.I., Horstwood, M.S.A., Pitfield, P.E.J., Gillespie, M., Darbyshire, F., O'Connor, E.A., Abdouloye, T.B., 2012. U-Pb dating and Sm–Nd isotopic analysis of granitic rocks from the Tiris Complex: New constaints on key events in the evolution of the Reguibat Shield, Mauritania. Precambrian Res. 204–205, 1–11. https://doi.org/10.1016/j.precamres.2011.12.008.
Tait, J., Straathof, G., Söderlund, U., Ernst, R.E., Key, R., Jowitt, S.M., Lo, K., Dahmada, M.E.M., N'Diaye, O., 2013. The Ahmeyim Great Dyke of Mauritania: a newly dated Archaean intrusion. Lithos 174, 323–332. https://doi.org/10.1016/j.lithos.2012.09.014.
Terentiev, R.A., Santosh, M., 2020. Baltica (East European Craton) and Atlantica (Amazonian and West African Cratons) in the Proterozoic: the pre-Columbia connection. Earth Sci. Rev. 210, 103378 https://doi.org/10.1016/j.earscirev.2020.103378.
Tikoff, B., Greene, D., 1997. Stretching lineations in transpressional shear zones: an example from the Sierra Nevada Batholith, California. J. Struct. Geol. 19, 29–39. https://doi.org/10.1016/S0191-8141(96)00056-9.
Traoré, K., Chardon, D., Naba, S., Wane, O., Bouaré, M.L., 2022. Paleoproterozoic collision tectonics in West Africa: insights into the geodynamics of continental growth. Precambr. Res. 376, 106692 https://doi.org/10.1016/j.precamres.2022.106692.
Ueda, K., Gerya, T.V., Burg, J.-P., 2012. Delamination in collisional orogens: Thermomechanical modeling. J. Geophys. Res. Solid Earth 117, 2012JB009144. https://doi.org/10.1029/2012JB009144.